Catalysis Communications 164 (2022) 106437

Contents lists available at ScienceDirect

Catalysis Communications

journal homepage: www.elsevier.com/locate/catcom

Mesoporous nano Ni-Al_2O_3 catalyst for CO_2 methanation in a continuously stirred tank reactor

Fanhui Meng [a,b,*], Lina Wang [a,b], Xin Li [b], Michal Perdjon [c], Zhong Li [a,b,*]

[a] State Key Laboratory of Clean and Efficient Coal Utilization, Taiyuan University of Technology, Taiyuan 030024, Shanxi, China
[b] Key Laboratory of Coal Science and Technology of Ministry of Education and Shanxi Province, Taiyuan University of Technology, Taiyuan 030024, China
[c] Centre for Doctoral Training in Catalysis, Cardiff Catalysis Institute, School of Chemistry, Cardiff University, Cardiff CF10 3AT, UK

ARTICLE INFO

Keywords:
CO_2 methanation
Mesoporous nano Ni-Al_2O_3
Synthetic natural gas
Pluronic P123
Continuously stirred tank reactor

ABSTRACT

Mesoporous nano Ni-Al_2O_3 catalysts were prepared by using Pluronic P123 (P123) and fatty alcohol polyoxyethylene ether (AEO-7) as structure directing agents (SDAs), and applied for CO_2 methanation in a continuously stirred tank reactor (CSTR). Compared with NiAl-A prepared by using AEO-7 as SDA and NiAl-N without SDA, NiAl-P prepared by using P123 as SDA possesses ordered mesopores, high Ni dispersion, large metal surface area and amounts of adsorbed CO_2, which benefits CO_2 conversion. Under the conditions of 1.0 MPa, 300 °C and H_2/CO_2 ratio of 4, NiAl-P shows the highest CO_2 conversion of 74.0% and CH_4 yield of 73.6%.

1. Introduction

In the past decades, the industrialization and urbanization across the world has resulted in a significant increase of CO_2 emissions, well known as main greenhouse gas leading to global warming [1,2]. The consequences of this global warming are mostly desertification, rising sea levels, and animal species extinction [2]. Therefore, the CO_2 mitigation and utilization are one of the most important challenges for modern societies [3,4]. The CO_2 capture and utilization technology, which capture the CO_2 and use it as feedstock to produce fuels, can play a significant role in CO_2 reduction, which is due to that the dependence of fossil fuels cannot be relieved in short term. The power-to-gas (PtG) route is regarded as a mature route because it can convert the intermittent renewable energy to synthetic natural gas [5–7]. In this concept, the captured CO_2 reacts with the H_2 originated from the water electrolysis by renewable energy, such as wind, solar or hydropower, to synthesize CH_4. Thus, the fluctuant renewable energy can be stored by the form of CH_4, which can be easily transported or injected into the existing gas pipelines [4]. Moreover, compared to other CO_2 conversion reactions like methanol, and dimethyl ether, CO_2 methanation possesses many advantages, such as high activity and selectivity and high energy efficiency [8].

Great efforts have been made to develop metal-based catalysts for CO_2 methanation in a fixed-bed reactor, for example, the Ni [4,9,10], Ru [11] and Rh [12] on various supports Al_2O_3 [9,13], SiO_2 [1,14], ZrO_2 [11], CeO_2 [15,16] and zeolite [4,17]. Among these, Al_2O_3 supported Ni catalysts possess high activity and CH_4 selectivity, and relatively low cost [4,13,18]. However, the thermodynamic analysis shows that CO_2 methanation ($CO_2 + 4H_2 \leftrightarrow CH_4 + 2H_2O$, $\Delta H_{298K} = -164$ kJ/mol) is highly exothermic [7,19], for every 1% CO_2 conversion, the temperature rise for a typical methanator gas composition in an ammonia plant is 60 °C [20]. The large amounts of released heat may cause catalyst sintering and carbon deposition, resulting in the decrease of CO_2 equilibrium conversion [1,7]. To solve the local overheating problem, one of the major challenges is to remove the highly exothermic heat in time. The continuously stirred tank reactor (CSTR) can be operated at a uniform temperature in the reaction process by using an inert liquid medium, such as liquid paraffin, to suspend catalyst, thus it is suitable for highly exothermic reactions [19,21,22]. Now, the CSTR has been widely used in many reactions, such as F-T synthesis [21,22] and methanol synthesis [23]. Recently, the studies on CO hydrogenation to CH_4 in a slurry-bed reactor have been reported [24–26].

It is known that physical and chemical properties of Ni-Al_2O_3 catalyst depends on catalyst preparation methods [27,28]. Compared with the conventional impregnation method, the one-pot evaporation induced self-assembly (EISA) method has attracted much attention due to its excellent property for material preparation and high dispersion of active metals [29–31]. Morris et al. [29] found that alumina-supported metal oxides *via* EISA method possess well-developed mesoporosity, relatively high BET surface area and large pore widths. For CO_2 methanation

* Corresponding authors at: No. 79 Yingze West Street, Taiyuan 030024, China.
E-mail addresses: mengfanhui@tyut.edu.cn (F. Meng), lizhong@tyut.edu.cn (Z. Li).

https://doi.org/10.1016/j.catcom.2022.106437
Received 26 September 2021; Received in revised form 9 February 2022; Accepted 21 February 2022
Available online 23 February 2022

reaction, it is well accepted that CO_2 is adsorbed on the support, then reacts with H_2 on the metal to produce CH_4. Thus, the physiochemical properties and Ni dispersion of Ni-Al_2O_3 are crucial for the reaction; moreover, since the inert liquid medium was adopted to suspend catalyst in CSTR, the catalysts with ordered mesoporous structure would benefit the mass transfer of feed gases and products [30]. Up to date, the reports of CO_2 methanation in a CSTR using Ni-Al_2O_3 catalyst have not been published before, which initiates the current work.

In this work, Ni-Al_2O_3 catalysts were prepared *via* EISA method using different structure directing agents (SDAs) to explore their physicochemical properties on CO_2 methanation in a CSTR. The catalysts were characterized by N_2 adsorption–desorption, X-ray diffraction (XRD), temperature-programmed reduction in H_2 (H_2-TPR), H_2-chemisorption, X-ray photoelectron spectroscopy (XPS), temperature-programmed desorption of CO_2 and NH_3 (CO_2-TPD and NH_3-TPD and transmission electron microscopy (TEM). The effects of reaction conditions, including stirring speed, reaction temperature, pressure, H_2/CO_2 molar ratio and gas hourly space velocity (GHSV) on CO_2 methanation performance were studied. The relationships between the CO_2 methanation activity and physicochemical properties of the catalysts were discussed.

2. Experimental

2.1. Catalyst preparation

Ni-Al_2O_3 catalyst was prepared by the method reported elsewhere [29]. Briefly, Pluronic P123 (P123) was dissolved in ethanol, then Al $(C_3H_7O)_3$, nitric acid and $Ni(NO_3)_2{\cdot}6H_2O$ were added in sequence. The mixed solution was stirred for 5 h and dried at 60 °C for 48 h. The obtained solid was calcined in air at 550 °C for 4 h, and denoted as NiAl-P. The sample NiAl-A was prepared by using AEO-7 as SDA. The sample NiAl-N prepared without SDA.

The content of Ni in Ni-Al_2O_3 was set at 30 wt%. All the calcined samples were crushed and grounded to 140–200 mesh particles before reduction. The reduction was carried out at 550 °C in 25%H_2/75%N_2 for 6 h. The detailed preparation description was supplied in Electronic Supporting Information (ESI).

2.2. Catalysts characterization

Ni-Al_2O_3 catalysts were characterized by powder and *in-situ* XRD, N_2 adsorption-desorption, TEM, H_2-TPR, XPS, H_2-chemisorption, CO_2-TPD and NH_3-TPD. The details of these characterizations were given in ESI.

2.3. Catalytic performance evaluation

The performance of CO_2 methanation was conducted in a CSTR. The gas products were analyzed by an online Agilent 7890A gas chromatography. CH_4 and C_{2-4} were analyzed by using FID equipped with HP-AL/S column. CO_2, N_2 and CO were analyzed by using TCD equipped with Porapak-Q column, PLOT/Q column and HP-MOLESIEVE column. The detailed reaction conditions and performance analysis were described in ESI.

3. Results and discussion

3.1. Textural properties

N_2 adsorption-desorption isotherms of calcined NiAl-P, NiAl-N and NiAl-A catalysts are displayed in Fig. 1(a). All samples exhibit typical type IV isotherms as defined by IUPAC classification, characteristic of the mesoporous structure. NiAl-P possesses an H1 type hysteresis loop, suggesting a uniform mesopores and a cylindrical mesopore channel among the framework [17]. NiAl-A catalyst, prepared by using AEO-7 as SDA, shows type IV curves with H3 type hysteresis loop, which is probably due to the non-rigid aggregation of plate-like particles. NiAl-N

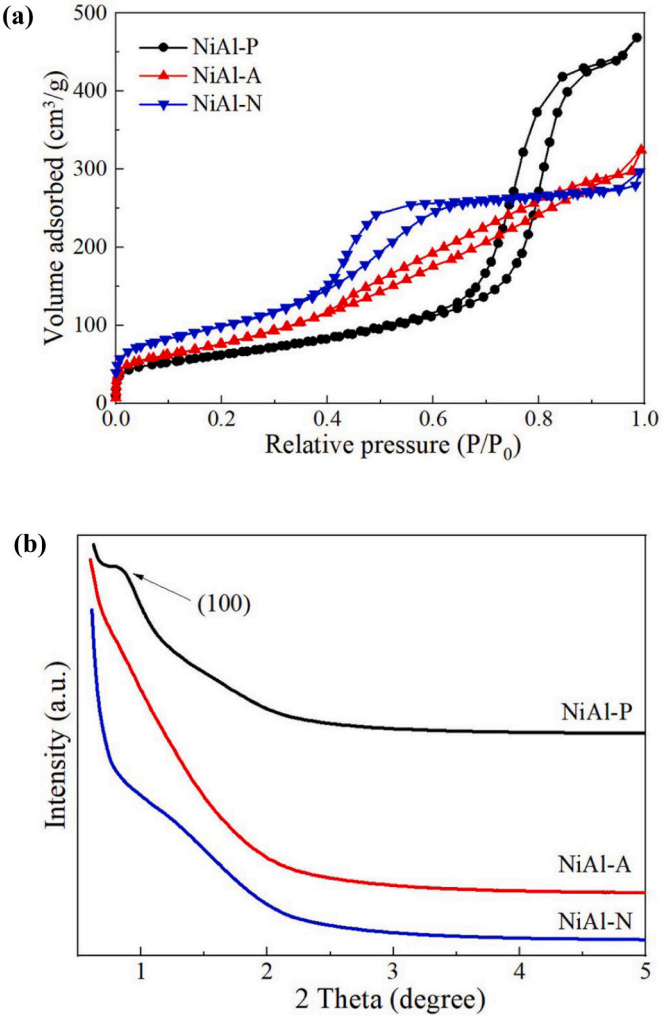

Fig. 1. (a) N_2 adsorption-desorption isotherms and (b) small-angle XRD patterns of calcined Ni-Al_2O_3 catalysts.

catalyst exhibits an H2 type hysteresis loop, which is the characteristic of mesopore with ink-bottle shaped pores. The pore size distributions of the samples are shown in Fig. S1. Obviously, NiAl-A and NiAl-N exhibit narrow peaks from 2 nm to 5 nm, whereas NiAl-P generates a broad pore size range from 6 nm to 12 nm. The textural properties of NiAl-P, NiAl-N and NiAl-A catalysts are listed in Table 1. NiAl-N sample shows slightly higher BET surface area than NiAl-A and NiAl-P samples. However, NiAl-P sample exhibits larger pore volume and average pore size than the NiAl-A and NiAl-N samples, which is due to the different SDAs in constructing the mesopore structure in the process of catalyst preparation.

3.2. Catalyst structure and morphology

The small-angle XRD patterns were selected to confirm the presence of ordered mesoporous structures of calcined Ni-Al_2O_3 catalysts. As shown in Fig. 1(b), NiAl-P catalyst presents an intense (100) peak at 0.9° and a weak one (110) around 1.4°, which is associated to the long-range and well-ordered mesoporous structure [32,33]. NiAl-A and NiAl-N catalysts do not display the characteristic peaks for mesoporous structures, the reason is probably due to the calcined SDA does not preserve the well-ordered mesopores.

The wide-angle XRD patterns of reduced Ni-Al_2O_3 catalysts are shown in Fig. S2. All samples exhibit the diffraction peaks of Ni metal at 2θ angle of 44.5°, 51.8° and 76.3° (JCPDS No. 47–1049). NiAl-N sample

Table 1
Textural properties, H_2-TPR and H_2-pulse chemisorption results of Ni-Al_2O_3 catalysts.

Catalysts	BET surface area (m^2/g)[a]	Pore volume (cm^3/g)[b]	Average pore diameter (nm)[c]	Ni crystallite size (nm)[d]	H_2 uptake (mmol/g)[e]	Reduction degree (%)[e]	Metal surface area (m^2/g_{cat})[f]	Dispersion (%)[f]
NiAl-P	298	1.13	6.79	6.2	4.91	96%	7.31	1.10
NiAl-A	292	0.61	4.95	6.4	3.96	77%	7.08	1.06
NiAl-N	362	0.58	4.80	10.4	2.75	54%	6.69	1.01

[a] Calculated by the BET equation.
[b] BJH desorption pore volume.
[c] BJH desorption average pore diameter.
[d] obtained from XRD results.
[e] obtained from H_2-TPR results.
[f] Determined from H_2 chemisorption by assuming that one hydrogen atom occupies one surface metallic Ni atom.

shows much higher diffraction peaks than the other two. The crystallite sizes of metallic Ni listed in Table 1 show that NiAl-P and NiAl-A exhibit much smaller Ni crystallite sizes than NiAl-N. The *in-situ* XRD patterns of NiAl-P catalyst in a H_2 atmosphere at various reduction temperature are shown in Fig. S3. As the reduction temperature lower than 450 °C, there is almost no diffraction peaks. However, increasing the reduction temperature to 500 °C, the peaks at 2θ of 44.5° and 51.8° corresponding to Ni metal appear and gradually intensify as the reduction temperature increases. The results suggest that 550 °C was enough for the catalyst reduction.

TEM images of calcined Ni-Al_2O_3 catalysts are displayed in Fig. 2. It can be seen that a contrast of NiO and Al_2O_3, the dark black particles are recognized as NiO particles, whereas the gray colored particles are Al_2O_3 [34]. All samples exhibit NiO particles, which is due to the high Ni content in Ni-Al_2O_3 catalysts. Even at this high Ni content, NiAl-P shows small and uniform particles size of NiO around 10 nm, and no obvious aggregation of large particles were observed, indicating the high dispersion of NiO particles. NiAl-A and NiAl-N catalysts exhibit large particles and obvious aggregation of NiO, consistent with the XRD results.

3.3. Catalyst surface properties

H_2-TPR was performed to determine the reducibility of Ni species and interaction between Ni and support, as shown in Fig. S4. NiAl-N and NiAl-A exhibit the reduction temperature at 516 °C and 585 °C, respectively, while NiAl-P exhibits the main reduction peaks at 627 °C and a shoulder peak appears at 543 °C, which is probably attributed to the reduction of NiO located outside the ordered channels. The TPR results indicate that NiAl-P exhibit a stronger interaction between NiO and Al_2O_3 than NiAl-N and NiAl-A. The amounts of H_2 consumption and NiO reduction degree are summarized in Table 1. It can be found that NiAl-P possesses the highest amount of H_2 consumption (4.91 mmol/g) and reduction degree (96%), while NiAl-N shows the lowest values. The H_2 pulse chemisorption data listed in Table 1 shows that NiAl-P exhibits the highest Ni metal surface area of 7.31 m^2/g_{cat} and highest Ni dispersion of 1.10%. NiAl-N exhibits the lowest values, which is attributed to the low reduction degree of Ni species.

XPS was performed to determine the chemical states of Ni species and interaction between Ni species and Al_2O_3. Fig. 3(a) shows the Ni $2p_{3/2}$ spectra of the reduced catalysts. The peaks at binding energies (B.E.s) of ~853.0 eV can be attributed to Ni^0 metal, while the peaks located around 856.2 eV indicates the presence of $NiAl_2O_4$ spinel (856.2 eV) [9,34]. It is worth to mention that NiAl-P and NiAl-A exhibit larger peak areas around 853.0 eV than NiAl-N, indicating the presence of larger amounts of Ni^0 on catalyst surface, consistent with the TPR analysis.

CO_2-TPD was performed to study the adsorption strength of CO_2 on Ni-Al_2O_3 catalysts, the profiles are shown in Fig. 3(b). Two desorption peaks are presented in the range of 50 ~ 200 °C and 200 ~ 350 °C. The peaks at low temperatures are attributed to the physical or weakly chemisorbed CO_2 on catalyst surface, while the peaks at high temperatures are ascribed to the strong basic sites on the catalyst surface [35].

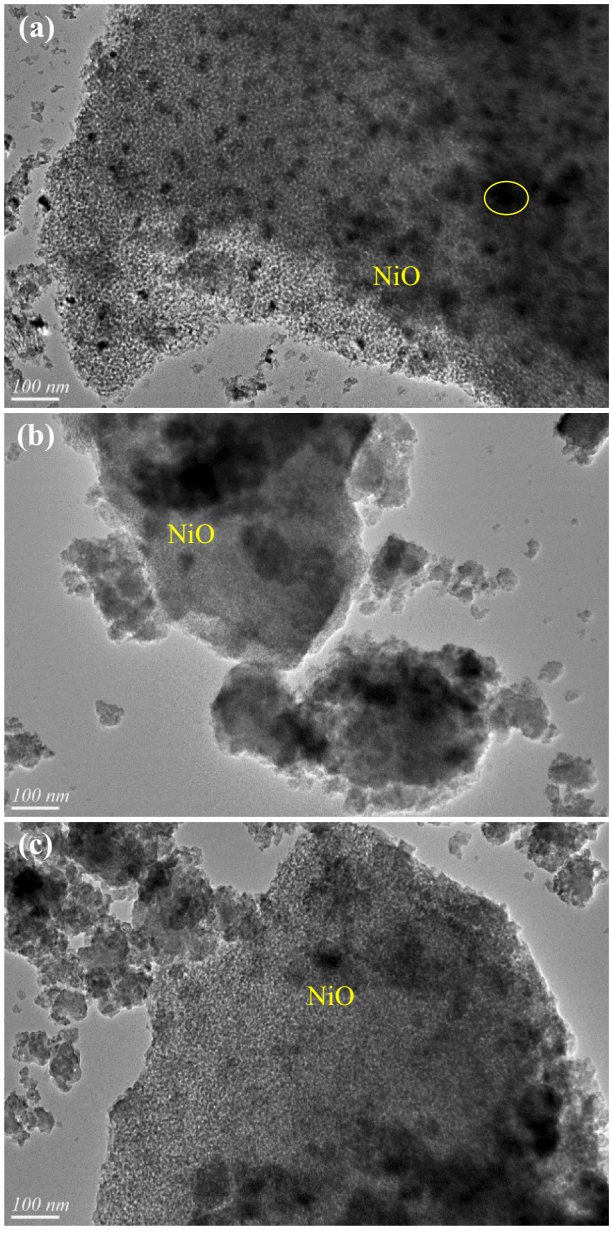

Fig. 2. TEM images of calcined Ni-Al_2O_3 catalysts. (a) NiAl-P, (b) NiAl-A, (c) NiAl-N.

NiAl-P shows a higher peak area and peak intensity at high temperature (~275 °C) than the other two, indicating that NiAl-P adsorbed more amounts of CO_2 benefiting the CO_2 conversion. NH_3-TPD profiles in

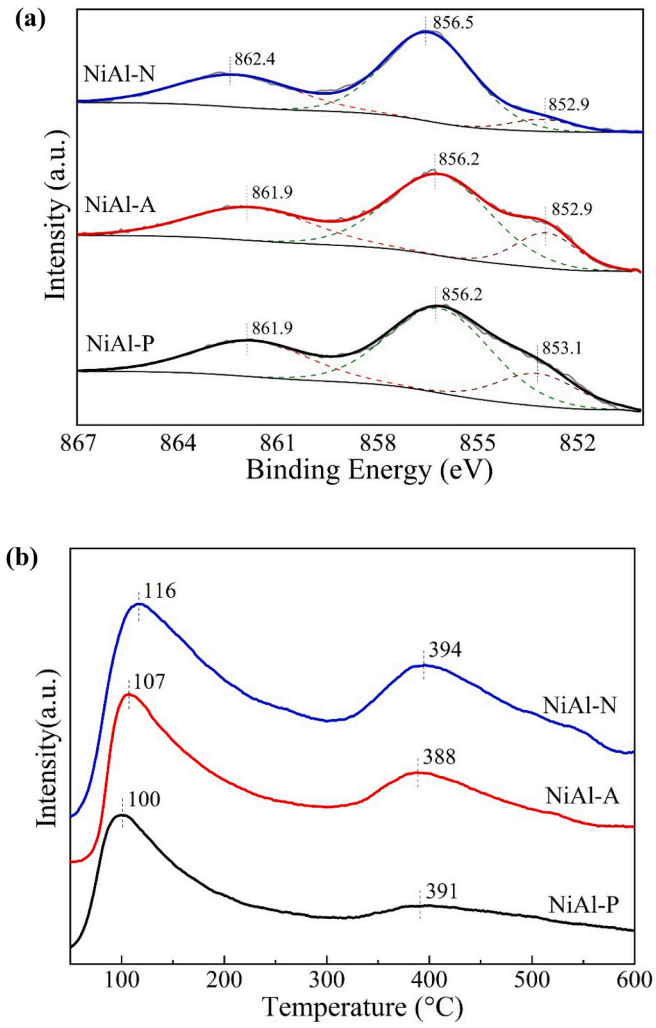

Fig. 3. (a) Ni $2p_{3/2}$ spectra and (b) CO_2-TPD profiles of reduced Ni-Al_2O_3 catalysts.

Fig. S5 shows that all samples exhibit two desorption peaks for NH_3. NiAl-N exhibits the largest desorption peaks at high temperature (~400 °C), which goes against the adsorption and conversion of CO_2. The results agree well with the CO_2-TPD analysis.

3.4. Catalyst performance for CO_2 methanation

The CO_2 methanation performance over Ni-Al_2O_3 catalyst was carried out in a CSTR. Before the evaluation, the reaction conditions were studied, including the stirring speed, reaction temperature, reaction pressure, H_2/CO_2 molar ratio and GHSV. The catalytic results are shown in Fig. S6. As shown in Fig. S6(a), the CO_2 conversion slightly increased as the stirring speed increased from 500 r/min to 800 r/min. Further increase the stirring speed, the CO_2 conversion does not change. It is suggested that the stirring speed of 800 r/min is enough to exclude the mass diffusion during the reaction. Fig. S6(b)–(d) show that CO_2 conversion increases as the reaction temperature (220–320 °C), pressure (0.5–3.0 MPa) or H_2/CO_2 ratio (2–5) increases. The increase of GHSV reduced the CO_2 conversion. Moreover, it is interesting to find that the reaction conditions do not changed the selectivity of CH_4 obviously. Thus, the performance tests of Ni-Al_2O_3 catalysts were carried out under the reaction conditions of 300 °C, 1.0 MPa, and 800 r/min with a H_2/CO_2 ratio of 4 and GHSV of 3000 mL/(g·h). The catalytic activity and stability are displayed in Fig. S7 and Table 2, respectively. It could be found in Fig. S7 that, after the catalyst induction period, all the catalysts exhibit high stability and selectivity for CH_4, C_{2-4} and CO. As shown in Table 2, NiAl-P catalyst exhibits the highest CO_2 conversion of 74.0% and CH_4 yield of 73.6%, while that of NiAl-N catalyst was only 57.5% and 57.0%, respectively. All the catalysts exhibit high selectivity for CH_4, and the selectivity of CO was only 0.2%. The high activity for NiAl-P catalyst was mainly attributed to the well-ordered mesopores, large Ni metal surface area, high Ni dispersion and amounts of adsorbed CO_2.

Table 2
Catalytic performance for CO_2 methanation over Ni-Al_2O_3 catalysts in a CSTR.

Catalyst	CO_2 conversion (%)	Selectivity (%)			CH_4 yield (%)
		CH_4	C_{2-4}	CO	
NiAl-P	74.0	99.5	0.3	0.2	73.6
NiAl-A	69.6	99.4	0.4	0.2	69.2
NiAl-N	57.5	99.1	0.7	0.2	57.0

4. Conclusions

Mesoporous nano Ni-Al_2O_3 catalysts were prepared by using different SDAs. The reaction conditions for CO_2 methanation in a CSTR including the stirring speed, reaction temperature, reaction pressure, H_2/CO_2 molar ratio and GHSV were studied. The catalytic performance shows that NiAl-P prepared by using P123 as SDA exhibits higher CO_2 conversion and CH_4 yield than those of NiAl-A and NiAl-N, which is due to that NiAl-P catalyst possesses ordered mesopores, high Ni dispersion, large metal surface area and amounts of adsorbed CO_2.

CRediT authorship contribution statement

Fanhui Meng: Conceptualization, Methodology, Writing – review & editing, Funding acquisition, Supervision. **Lina Wang:** Investigation. **Xin Li:** Investigation, Data curation. **Michal Perdjon:** Investigation. **Zhong Li:** Conceptualization, Funding acquisition, Supervision.

Declaration of Competing Interest

The authors declare that they have no known competing financial interests or personal relationships that could have appeared to influence the work reported in this paper.

Acknowledgements

This work was financially supported by Natural Science Foundation of Shanxi Province (201801D121056), the Key Research and Development Project of Shanxi Province (201803D421011), and National Natural Science Foundation of China (U1510203).

Appendix A. Supplementary data

Supplementary data to this article can be found online at https://doi.org/10.1016/j.catcom.2022.106437.

References

[1] R. Ye, L. Liao, T.R. Reina, J. Liu, D. Chevella, Y. Jin, M. Fan, J. Liu, Engineering Ni/SiO_2 catalysts for enhanced CO_2 methanation, Fuel 285 (2021), 119151, https://doi.org/10.1016/j.fuel.2020.119151.
[2] I. Martínez-Zarzoso, A. Maruotti, The impact of urbanization on CO_2 emissions: evidence from developing countries, Ecol. Econ. 70 (2011) 1344–1353, https://doi.org/10.1016/j.ecolecon.2011.02.009.
[3] W. Li, Y. Liu, M. Mu, F. Ding, Z. Liu, X. Guo, C. Song, Organic acid-assisted preparation of highly dispersed co/ZrO_2 catalysts with superior activity for CO_2 methanation, Appl. Catal. B Environ. 254 (2019) 531–540, https://doi.org/10.1016/j.apcatb.2019.05.028.
[4] Y. Chen, B. Qiu, Y. Liu, Y. Zhang, An active and stable nickel-based catalyst with embedment structure for CO_2 methanation, Appl. Catal. B Environ. (2020), 118801, https://doi.org/10.1016/j.apcatb.2020.118801.

[5] A. Ricca, L. Truda, V. Palma, Study of the role of chemical support and structured carrier on the CO_2 methanation reaction, Chem. Eng. J. 377 (2019), 120461, https://doi.org/10.1016/j.cej.2018.11.159.
[6] Y. Chen, W. Bi, L. Chen, Q. Liu, Urea-assisted synthesis towards a renewable rice husk silica-derived Ni-phyllosilicate catalyst for CO_2 methanation, Int. J. Hydrog. Energy 46 (2021) 27567–27575, https://doi.org/10.1016/j.ijhydene.2021.06.035.
[7] L. Shen, J. Xu, M. Zhu, Y. Han, Essential role of the support for nickel-based CO_2 methanation catalysts, ACS Catal. 10 (2020) 14581–14591, https://doi.org/10.1021/acscatal.0c03471.
[8] P. Hongmanorom, J. Ashok, G. Zhang, Z. Bian, M.H. Wai, Y. Zeng, S. Xi, A. Borgna, S. Kawi, Enhanced performance and selectivity of CO_2 methanation over phyllosilicate structure derived Ni-Mg/SBA-15 catalysts, Appl. Catal. B Environ. 282 (2021), 119564, https://doi.org/10.1016/j.apcatb.2020.119564.
[9] G. Garbarino, P. Kowalik, P. Riani, K. Antoniak-Jurak, P. Pieta, A. Lewalska-Graczyk, W. Lisowski, R. Nowakowski, G. Busca, I.S. Pieta, Improvement of Ni/Al_2O_3 catalysts for low-temperature CO_2 methanation by vanadium and calcium oxide addition, Ind. Eng. Chem. Res. 60 (2021) 6554–6564, https://doi.org/10.1021/acs.iecr.0c05556.
[10] Y. Wu, J. Lin, G. Ma, Y. Xu, J. Zhang, C. Samart, M. Ding, Ni nanocatalysts supported on mesoporous Al_2O_3–CeO_2 for CO_2 methanation at low temperature, RSC Adv. 10 (2020) 2067–2072, https://doi.org/10.1039/C9RA08967E.
[11] S. Chen, A.M. Abdel-Mageed, M. Li, S. Cisneros, J. Bansmann, J. Rabeah, A. Brückner, A. Groß, R. Jürgen Behm, Electronic metal-support interactions and their promotional effect on CO_2 methanation on Ru/ZrO_2 catalysts, J. Catal. 400 (2021) 407–420, https://doi.org/10.1016/j.jcat.2021.06.028.
[12] Y. Jiang, J. Lang, X. Wu, Y.H. Hu, Electronic structure modulating for supported Rh catalysts toward CO_2 methanation, Catal. Today 356 (2020) 570–578, https://doi.org/10.1016/j.cattod.2020.01.029.
[13] N. Schreiter, J. Kirchner, S. Kureti, A DRIFTS and TPD study on the methanation of CO_2 on Ni/Al_2O_3 catalyst, Catal. Commun. 140 (2020), 105988, https://doi.org/10.1016/j.catcom.2020.105988.
[14] K. Wang, Y. Men, S. Liu, J. Wang, Y. Li, Y. Tang, Z. Li, W. An, X. Pan, L. Li, Decoupling the size and support/metal loadings effect of Ni/SiO_2 catalysts for CO_2 methanation, Fuel 304 (2021), 121388, https://doi.org/10.1016/j.fuel.2021.121388.
[15] G. Varvoutis, M. Lykaki, S. Stefa, E. Papista, S.A.C. Carabineiro, G.E. Marnellos, M. Konsolakis, Remarkable efficiency of Ni supported on hydrothermally synthesized CeO_2 nanorods for low-temperature CO_2 hydrogenation to methane, Catal. Commun. 142 (2020), 106036, https://doi.org/10.1016/j.catcom.2020.106036.
[16] N. Rui, X. Zhang, F. Zhang, Z. Liu, X. Cao, Z. Xie, R. Zou, S.D. Senanayake, Y. Yang, J.A. Rodriguez, C. Liu, Highly active Ni/CeO_2 catalyst for CO_2 methanation: preparation and characterization, Appl. Catal. B Environ. 282 (2021), 119581, https://doi.org/10.1016/j.apcatb.2020.119581.
[17] S.N. Bukhari, C.C. Chong, H.D. Setiabudi, Y.W. Cheng, L.P. Teh, A.A. Jalil, Ni/fibrous type SBA-15: highly active and coke resistant catalyst for CO_2 methanation, Chem. Eng. Sci. 229 (2021), 116141, https://doi.org/10.1016/j.ces.2020.116141.
[18] A. Cárdenas-Arenas, A. Quindimil, A. Davó-Quiñonero, E. Bailón-García, D. Lozano-Castelló, U. De-La-Torre, B. Pereda-Ayo, J.A. González-Marcos, J. R. González-Velasco, A. Bueno-López, Isotopic and in situ DRIFTS study of the CO_2 methanation mechanism using Ni/CeO_2 and Ni/Al_2O_3 catalysts, Appl. Catal. B Environ. 265 (2020), 118538, https://doi.org/10.1016/j.apcatb.2019.118538.
[19] J. Lefebvre, S. Bajohr, T. Kolb, A comparison of two-phase and three-phase CO_2 methanation reaction kinetics, Fuel 239 (2019) 896–904, https://doi.org/10.1016/j.fuel.2018.11.051.
[20] G. Zhang, T. Sun, J. Peng, S. Wang, S. Wang, A comparison of Ni/SiC and Ni/Al_2O_3 catalyzed total methanation for production of synthetic natural gas, Appl. Catal. A 462-463 (2013) 75–81, https://doi.org/10.1016/j.apcata.2013.04.037.
[21] W. Hou, B. Wu, Y. Yang, Q. Hao, L. Tian, H. Xiang, Y. Li, Effect of SiO_2 content on iron-based catalysts for slurry Fischer–Tropsch synthesis, Fuel Process. Technol. 89 (2008) 284–291, https://doi.org/10.1016/j.fuproc.2007.11.031.
[22] Y. Liu, T. Hanaoka, T. Miyazawa, K. Murata, K. Okabe, K. Sakanishi, Fischer–Tropsch synthesis in slurry-phase reactors over Mn- and Zr-modified Co/SiO_2 catalysts, Fuel Process. Technol. 90 (2009) 901–908, https://doi.org/10.1016/j.fuproc.2009.04.004.
[23] L.H. Hu, X.J. Wang, G.S. Yu, F.C. Wang, Z.H. Yu, Study of the characteristics of methanol synthesis in a recirculation slurry reactor – a novel three-phase synthesis reactor, Chem. Eng. Technol. 31 (2008) 33–37, https://doi.org/10.1002/ceat.200700081.
[24] J. Zhang, Y. Bai, Q. Zhang, X. Wang, T. Zhang, Y. Tan, Y. Han, Low-temperature methanation of syngas in slurry phase over Zr-doped Ni/γ-Al_2O_3 catalysts prepared using different methods, Fuel 132 (2014) 211–218, https://doi.org/10.1016/j.fuel.2014.04.085.
[25] F. Meng, Z. Li, J. Liu, X. Cui, H. Zheng, Effect of promoter Ce on the structure and catalytic performance of Ni/Al_2O_3 catalyst for CO methanation in slurry-bed reactor, J. Nat. Gas Sci. Eng. 23 (2015) 250–258, https://doi.org/10.1016/j.jngse.2015.01.041.
[26] Y. Gao, F. Meng, Y. Cheng, Z. Li, Influence of fuel additives in the urea-nitrates solution combustion synthesis of Ni-Al_2O_3 catalyst for slurry phase CO methanation, Appl. Catal. A Gen. 534 (2017) 12–21, https://doi.org/10.1016/j.apcata.2017.01.016.
[27] B. Lu, K. Kawamoto, Preparation of the highly loaded and well-dispersed NiO/SBA-15 for methanation of producer gas, Fuel 103 (2013) 699–704, https://doi.org/10.1016/j.fuel.2012.09.009.
[28] L. Xu, F. Wang, M. Chen, J. Zhang, K. Yuan, L. Wang, K. Wu, G. Xu, W. Chen, CO_2 methanation over a Ni based ordered mesoporous catalyst for the production of synthetic natural gas, RSC Adv. 6 (2016) 28489–28499, https://doi.org/10.1039/C6RA01139J.
[29] S.M. Morris, P.F. Fulvio, M. Jaroniec, Ordered mesoporous alumina-supported metal oxides, J. Am. Chem. Soc. 130 (2008) 15210–15216, https://doi.org/10.1021/ja806429q.
[30] L. Xu, H. Song, L. Chou, Ordered mesoporous MgO–Al_2O_3 composite oxides supported Ni based catalysts for CO_2 reforming of CH_4: effects of basic modifier and mesopore structure, Int. J. Hydrog. Energy 38 (2013) 7307–7325, https://doi.org/10.1016/j.ijhydene.2013.04.034.
[31] Q. Liu, Z. Zhong, F. Gu, X. Wang, X. Lu, H. Li, G. Xu, F. Su, CO methanation on ordered mesoporous Ni–Cr–Al catalysts: effects of the catalyst structure and Cr promoter on the catalytic properties, J. Catal. 337 (2016) 221–232, https://doi.org/10.1016/j.jcat.2016.01.023.
[32] J. Liu, W.L. Shen, D.M. Cui, J. Yu, F.B. Su, G.W. Xu, Syngas methanation for substitute natural gas over Ni-Mg/Al_2O_3 catalyst in fixed and fluidized bed reactors, Catal. Commun. 38 (2013) 35–39, https://doi.org/10.1016/j.catcom.2013.04.014.
[33] H. Ai, Q. Liu, H. Yang, W-doped ordered mesoporous Ni–Al_2O_3 catalyst for methanation of carbon monoxide, Int. J. Hydrog. Energy 44 (2019) 23975–23982, https://doi.org/10.1016/j.ijhydene.2019.07.115.
[34] F. Meng, X. Li, M. Li, X. Cui, Z. Li, Catalytic performance of CO methanation over La-promoted Ni/Al_2O_3 catalyst in a slurry-bed reactor, Chem. Eng. J. 313 (2017) 1548–1555, https://doi.org/10.1016/j.cej.2016.11.038.
[35] M. Tan, X. Wang, X. Wang, X. Zou, W. Ding, X. Lu, Influence of calcination temperature on textural and structural properties, reducibility, and catalytic behavior of mesoporous γ-alumina-supported Ni–Mg oxides by one-pot template-free route, J. Catal. 329 (2015) 151–166, https://doi.org/10.1016/j.jcat.2015.05.011.